Mon. Not. R. astr. Soc. (1987) **225,** 307–327

Variations in the spectral index of the galactic radio continuum emission in the northern hemisphere

K. D. Lawson, C. J. Mayer, J. L. Osborne and M. L. Parkinson *Department of Physics, University of Durham, South Road, Durham DH1 3LE*

Accepted 1986 September 30. Received 1986 September 17

Summary. A study is made of the radio continuum emission of the Galaxy in the North Celestial Hemisphere. The variation of spectral index over a range of frequencies between 38 and 1420 MHz is derived after consideration of the accuracy of the temperature scales and zero levels of the surveys. Comparison with the results of earlier low-resolution surveys made with scaled arrays or horns lends support to the procedure adopted for the fixing of base levels. Most of the features with large angular scales appear to be associated with the radio loops I and III even at considerable angular distances from their ridge lines. This casts some doubt on earlier deductions of the properties of a galactic halo from low-resolution surveys. The spectral index variation of the radio loops is discussed in the context of diffusive shock acceleration of cosmic ray electrons. It is suggested that the steepening of the spectrum is best accounted for if there is an upper energy limit to the shock acceleration in the loops in the region of 5–10 GeV.

1 Introduction

The radio continuum emission of the Galaxy consists of synchrotron radiation from cosmic ray electrons and bremsstrahlung emission from thermal electrons. Up to frequencies of several GHz the synchrotron radiation dominates, this domination being essentially complete for directions more than a few degrees from the Galactic plane. Thus radio surveys provide information on cosmic ray electrons in the range 0.1 to 10 GeV distributed throughout the Galaxy. The spectral index of the synchrotron emission is directly related to that of the energy spectrum of cosmic ray electrons. The spatial distribution of the electrons and variations in their energy spectrum are important data to consider in the investigation of their acceleration and propagation in the Galaxy. In this paper we make a detailed study of variation of the spectral index of the Galactic continuum emission from that part of the Galaxy seen in the North Celestial Hemisphere.

In Section 2 we describe in some detail the surveys we have used, in order of increasing frequency from 38 to 1420 MHz. In deriving spectral indices from the comparison of observations

at different frequencies it is very important to take into account the accuracy with which the temperature scales and the zero levels of the surveys have been determined. Other points to be considered are the contributions from such sources as atmospheric emission, ground radiation and Galactic radiation in the sidelobes of the telescope.

After convolution of the pairs of surveys to common resolutions and subtraction of estimated extragalactic contributions, the spectral index distributions over the Northern Hemisphere are derived in Section 3. This extends the work of Kallas, Reich & Haslam (1983) which was concerned with the spectral index between 408 and 1420 MHz for the Cassiopeia–Perseus region within 10° of the Galactic plane.

In Section 4 the variations of spectral index arrived at in Section 3 are compared with the results of earlier work. Most of this was done using scaled arrays or horns which had considerably lower angular resolution. It is interesting to see how these results fit into the more detailed picture. The design of some of the earlier experiments was such that the effects of errors on the base levels and the extraneous contributions to the brightness temperature were largely removed. The comparison thus gives a check on the procedure used for dealing with these effects in Section 3. We consider also the validity of the derivation of the properties of a Galactic radio halo from the low-resolution scans.

An interpretation of the spectral index distribution is given in Section 5. It is suggested that most of the large angular scale features in the distribution are associated with the radio loops I and III. Models of the loops in the context of diffusive shock acceleration of cosmic ray electrons are discussed.

Conclusions are drawn in Section 6 where suggestions for further investigations are made.

2 Observations

Large-scale surveys of the Galactic continuum radiation have been completed over a wider range of frequencies in the Northern Hemisphere than in the south. The present study is therefore restricted to the Northern Hemisphere. We consider the surveys in order of increasing frequency.

Each survey gives the intensity, I, of the radiation at a frequency, f, as a function of position on the sky. The intensity is usually expressed in terms of the brightness temperature, T_b, by

$$T_b=(c^2/2kf^2)I\equiv 3.25\times 10^{-5}I/f^2 \qquad (2.1)$$

where T_b is in K, I is in Jy sr^{-1} and f is in GHz.

2.1 38 MHz

A survey at 38 MHz was made in 1967 with the 75-m Jodrell Bank Mark I telescope (Milogradov-Turin & Smith 1973; Milogradov-Turin 1984). The first publication covers the declination range $-25°<\delta<70°$ and the second gives the data for the polar cap. The beam pattern was directly measured with the aid of the Mark III telescope and a dipole transmitter. The half-power beamwidth (henceforward referred to simply as the beamwidth) was 7° in RA by 8° in Dec. The proportion of the power in the main beam out to 10° was 83 per cent and in the sidelobes 17 per cent. The telescope was used as a transit instrument fixed on the meridian. Two strips of declination 5° apart were completed each day by stepping from one to the other every 8 min. To check the zero level the telescope was occasionally directed at the North Celestial Pole and some runs were made through the whole range of declination. The left-hand circularly polarized component was recorded but, since the net circular polarization of the continuum is zero, the equivalent total intensity was obtained.

The calibration of the antenna temperature by means of a standard diode noise source was

believed to be correct to 5 per cent. The internal consistency of the measurements amounted to the larger of 300 K or 5 per cent. The sidelobes were expected to give an error generally much less than 10 per cent and reflected radiation did not exceed 2 per cent.

We digitized the maps of Milogradov-Turin & Smith and then applied their correction curves for ionospheric absorption (the maximum correction, at $\delta=0°$, is 9 per cent). The resulting distribution of brightness temperature for the Northern Hemisphere is shown in Fig. 1(a). There are two hatched regions at high declinations where the survey is incomplete. In this and subsequent maps we have used a stereographic projection. This has the property that all circular features on the sky (e.g. lines of latitude and longitude and the ridge lines of Loops I and III) project as arcs of circles.

2.2 178 MHz

The long element of the radio interferometer used in the Cambridge 4C survey was employed by Turtle & Baldwin (1962) in a survey at 178 MHz. The antenna was a parabolic cylinder 442 m long oriented in the east–west direction. It had a width of 20 m and could be rotated about the east–west axis over the declination range $-5°<\delta<90°$. Drift scans for 24 hr of RA were made at intervals of 3° in Dec over this range, each scan being repeated at least once.

Daily calibrations of the temperature scale were made against a noise diode. For repeated observations the zero levels varied by up to 20 K. The results were reduced to an arbitrary common zero level by comparison with a special series of observations which covered the whole range of Dec at 90^m intervals of RA. In order to determine the absolute zero level and check the temperature scale, a point-by-point comparison was made with the low-resolution survey at the same frequency by Turtle *et al.* (1962) (see Section 4) after both surveys had been convolved to a common resolution. As a result the zero level was determined to within ±10 K and the temperature scale to 5 per cent.

The beamwidth of the antenna was 4°.6 in Dec and 13′.4 in RA. Over most of the sky the brightness temperature recorded was the mean taken over successive 5^m intervals of RA. The shape of the beam in declination was such that, for isotropic radiation, 33 per cent would fall in the sidelobes. Corrections to the observed brightness temperature were therefore necessary for Galactic and ground radiation in the sidelobes. To do this the authors made a one-dimensional convolution of the observed brightness temperature which broadened the beam to 5° but reduced the sidelobe contribution to 1 per cent. The effect of this is to produce a map showing greater contrast in brightness temperature. The changes amounted to approximately 25 per cent of the difference from the mean level of the map (220 K). For example, the minimum sky brightness is 76 K after the original value has been reduced by 30 K. (The magnitude of this correction is discussed further in Section 3.) In view of the uncertainties in the correction procedure the quoted uncertainty in the zero level of the survey was increased to ±15 K. Fig. 1(b) shows a stereographic projection that we have produced from digitized data supplied to us.

2.3 404 MHz

Pauliny-Toth & Shakeshaft (1962) measured the brightness temperature of the sky in the declination range $-20°<\delta<90°$ with a 7.5-m paraboloid having a beam width of 8°.5×6°.5. This was an absolutely calibrated survey. Although we do not use it directly in our derivation of the spectral index it formed the basis for the calibration of the 408-MHz survey described in the next section so we give some details here.

The brightness temperature was determined for a grid of points spaced by between 10° and 15°. Most of the observations were made at transit. The spacing means that the sky was undersampled

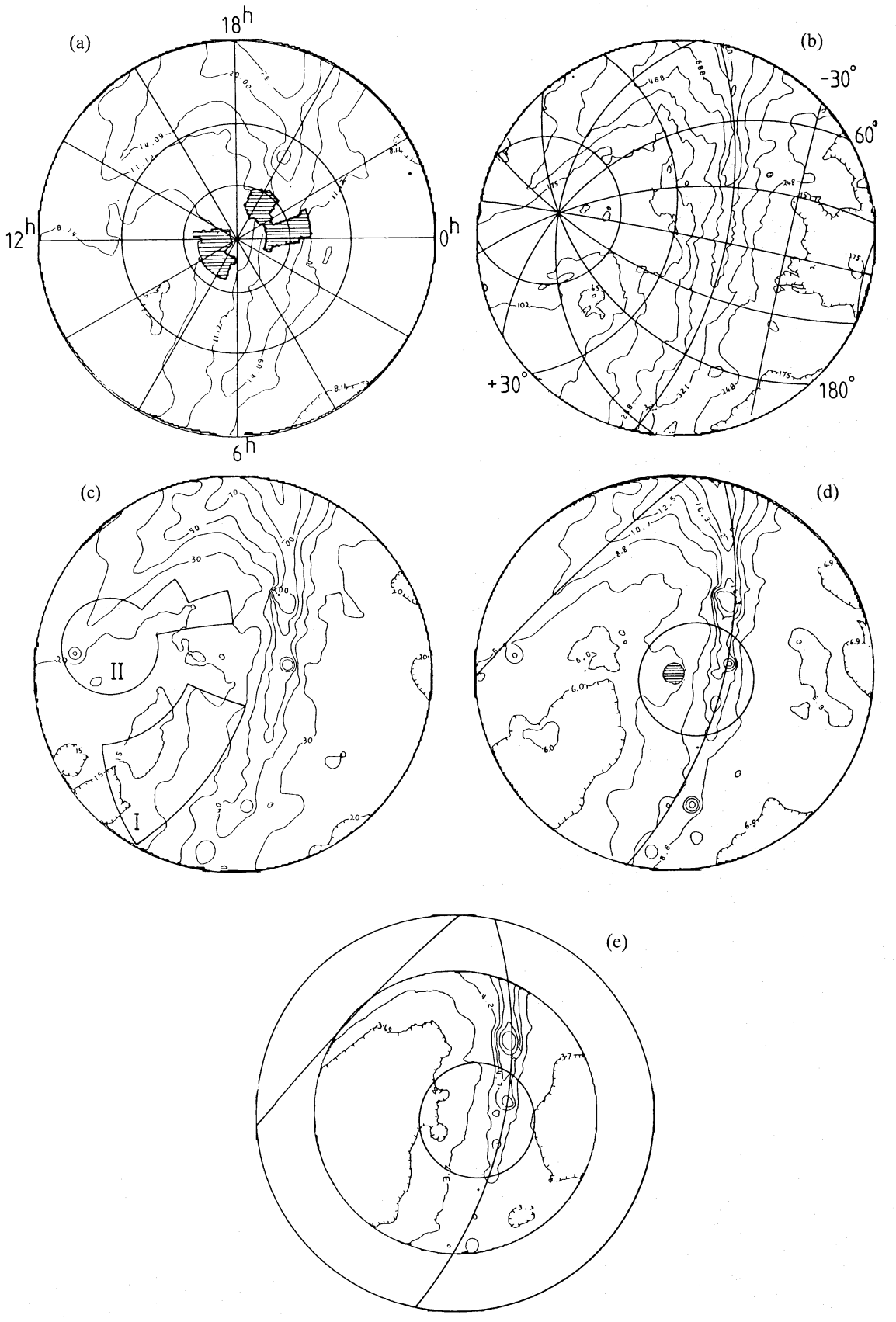

and that comparison with other frequencies should be made at the specific points rather than via the published contour map. The procedure adopted was first to determine the temperatures of the grid points with respect to that of the North Celestial Pole and then to find the pole temperature from a separate series of measurements. The noise power of the aerial was compared with that from a resistance immersed in liquid nitrogen. The error in the calibration of the temperature scale was ±2 per cent. Taking into account the uncertainties in the corrections described below the brightness temperature of the North Celestial Pole was found to be 23.9±2.0 K.

After allowance had been made for the loss factor of the feed, contributions to the aerial temperature from the ground and the atmosphere had to be subtracted. From measurements of the change in brightness temperature of several regions of the sky as their elevations varied, the ground and atmospheric contributions were determined relative to their values at the zenith. At these wavelengths the main part of the atmospheric attenuation is due to non-resonant absorption by molecular oxygen. The fraction absorbed is <1 per cent but the corresponding atmospheric emission is important because the temperature of the atmosphere (about 260 K) is much greater than the brightnesss temperature of the Galactic emission. The contribution from the ground, when the telescope was pointed at the zenith, was calculated from the measured reception pattern of the aerial and the atmospheric contribution was calculated from the attenuation given by Hogg (1959). The summed zenithal contribution amounted to 2 K and the measured variation with elevation agreed well with that predicted. The final correction was to remove the contribution of the sidelobes in order to obtain the main beam aerial temperature which leads directly to the brightness temperature of the sky convolved over the near-Gaussian main beam of the aerial. The measured reception pattern, which had 85 per cent of the power in the main beam and 15 per cent in the sidelobes, was folded in by a series of successive approximations to the distribution of brightness temperature over the sky. The maximum difference between the full-beam aerial temperature and the final brightness temperature was 12 per cent, near to the Galactic plane.

Uncertainties in the various corrections lead to an overall absolute error of ±2.3 K and a temperature scale error of ±3.6 per cent.

2.4 408 MHz

The only all-sky survey of the Galactic continuum radiation in which the component parts were all done at the same frequency using telescopes with similar beamsize and a common data gathering

---

Figure 1. Contour maps of brightness temperature over the Northern Hemisphere. A stereographic projection is used, centred on the North Pole. In this projection the normalized radial coordinate, r, and the declination, δ, are related by $r=\tan(45°-\delta/2)$. The eight contour levels at each frequency have been chosen so that if the Galactic emission had a uniform spectral index, $\beta=2.4$, the maps would be identical. (On some of the maps fewer than eight levels are plotted because there are no points below the lowest level in the set or above the highest level. In this case the unplotted levels are given in brackets.) (a) 38 MHz. Contour levels, in units of 1000 K, are (3.67), 5.16, 8.14, 11.12, 14.09, 20, 29 and (59). The grid shows right ascension and declination at 30° intervals. (b) 178 MHz. Contour levels, in units of K, are 65, 102, 175, 248, 321, 468, 688 and 1420. The grid shows Galactic latitude and longitude at 30° intervals. (c) 408 MHz convolved to a resolution of 4°. Contour levels, in units of K, are 15, 20, 30, 40, 50, 70, 100 and 200. Regions I, 'the local spiral arm', and II, 'the interarm', of Bridle (1967) are marked. (d) 820 MHz convolved to a resolution of 4°. Contour levels, in units of K, are 6.0, 6.9, 8.8, 10.7, 12.5, 16.3, 21.9 and 40.6. Here and in (e) the arc of $b=0°$ is shown together with the arc of loop I and the circle of loop III as fitted by Berkhuijsen, Haslam & Salter (1971). (e) 1420 MHz convolved to a resolution of 4°. Contour levels, in units of K, are 3.45, 3.7, 4.2, 4.7, 5.2, 6.2, 7.7 and (12.7). Data plotted are for part 1 of the survey which extends down to 20° only.

and reduction procedure is that of Haslam *et al.* (1982). The parts of the survey, in the order of which they were done are as follows. Part 1 (Haslam, Quigley & Salter 1970) used the Mark I Jodrell Bank Telescope to cover the RA range $0^h<\alpha<4^h$ for $20°<\delta<60°$ and the range $4^h<\alpha<12^h$ for $-20°<\delta<60°$. Part 2 (Haslam *et al.* 1974) used the Effelsberg 100-m telescope for the remaining northern sky for $-8°<\delta<48°$. Part 3 covered the entire southern sky with the Parkes 64-m telescope (beamwidth 51 arcmin) and part 4 filled in the North Polar Cap ($\delta>45°$) by use of the Jodrell Bank Mark IA Telescope. Parts 3 and 4 are described by Haslam *et al.* (1981). We discuss part 3 no further. The left-hand circularly polarized component was measured.

Practically all of the measurements were made using the 'nodding scan' technique in which the telescope is fixed at the azimuth of the meridian and is driven at a constant rate between the prescribed declination limits while the rotation of the Earth provides the coverage in RA. For parts 1, 2 and 4 the fixed scan rate lay between 3° and 4° min^{-1}. There was an offset of the starting time of scans on successive days such that the scan lines were separated by rather less than half of the beamwidth. This technique leads to each downward scan being crossed at frequent regular intervals by an upward scan and allows a consistent zero level to be set by a system of minimizing the errors. The final residual baseline error for each scan was <1.5 K.

The absolute zero level and brightness temperature for parts 1, 2 and 4 of the survey were determined by reference to the 404-MHz survey of Pauliny-Toth & Shakeshaft (1962). The 408-MHz measurements were convolved to the 404-MHz beam shape and the latter temperatures were scaled to 408 MHz using a spectral index of 2.5. At each 10° of declination the best straight-line fit was found for the plot of one survey's data against the other. The slope of the line then gives the brightness temperature scale and the intercept the zero level correction at that declination. As all measurements were made at transit, a given declination corresponds to a fixed elevation and the elevation-dependent contributions of the atmosphere and ground radiation are automatically eliminated by this procedure. The combination of the errors of the straight-line fits with those of the 404-MHz survey lead to an error in the absolute zero level of ± 3 K and in the temperature scale of ± 10 per cent.

The beam pattern for each of the northern parts of the survey were investigated by making a series of scans through the bright radio source Cas A. In part 1 of the survey the main beam was an elliptical Gaussian of width 44×47 $arcmin^2$. Parts 2 and 4 had circular Gaussian main beams of width 37 and 49 arcmin, respectively. When the parts were combined to form the all-sky survey they were convolved to a common beam width of 51 arcmin. The form of the sidelobe response was also measured. For part 2 of the survey, for instance, the power in the sidelobes out to 5° was less than 5 per cent of that in the main beam. No correction was made for the sidelobes and it was argued that the excellent agreement in the overlap region between parts of the survey made with different telescopes suggests the absence of major distortions of the brightness temperature distribution.

It should be noted that when parts 1 and 2 were combined they were recalibrated against the 404-MHz measurements and small corrections ($\simeq 1$ K) were made to their base levels and scales. When we studied the spectral index distribution derived from the 408 and 1420 MHz surveys it was apparent that there was a small but distinct step in the index across the join between parts 2 and 4 of the 408 MHz survey. It was found by trial that subtracting 1.7 K, which is well within the quoted zero level error, from the whole of part 4 gave the smoothest join. Using these corrected brightness temperatures for the North Polar Cap, we simulated the Howell & Shakeshaft (1967) horn measurement of the pole temperature by convolving to the theoretical beam shape of the horn antenna (beam width $\simeq 15°$). The simulated value of 24.3 K agrees exactly with the observed one, for which an error of ± 0.9 K is quoted. We therefore have applied this correction to the published 408-MHz survey in the following analysis. Fig. 1(c) shows the 408-MHz map of the Northern Hemisphere.

2.5 820 MHz

A survey covering the declination range $-7°<\delta<85°$ at 820 MHz was made by Berkhuijsen (1972) using the Dwingeloo 25-m telescope. The beamwidth of the antenna was 1°.0 but regridding of the data increased the effective beamwidth to 1°.2. Crossed dipoles recorded the total intensity of the radiation.

In order to keep the atmospheric and ground radiation contributions approximately constant, scans were made in azimuth at elevations of 52°.8 (that of the North Celestial Pole), 40° and 26°. Azimuth ranges were chosen to give an overlap in declination of several degrees between adjacent elevations. The telescope scanned in azimuth at 2°.5 min^{-1} at the lower elevations and at 5° min^{-1} at the highest elevation. Except for three small strips the survey was fully sampled with two or more data points per beamwidth.

The full-beam pattern of the antenna was determined from scans across Cass A and the Sun. The sidelobe pattern outside the full beam was measured using a test transmitter. A correction to this pattern was indicated when the total antenna solid angle was deduced from observations of three bright radio point sources of known flux density. The sidelobe solid angle was 13 per cent of the total antenna solid angle. The correction for radiation in the sidelobes was calculated by scaling a earlier 408-MHz survey to 820 MHz using a spectral index of 2.4 within 10° of the Galactic plane and 2.7 elsewhere. The elevation-dependent contributions of the ground radiation and atmospheric emission were also calculated. For the latter the zenithal extinction was needed. The value at 820 MHz by Hogg (1959) is 0.028 dB. In contrast, direct determination of the extinction by tracking a source as its elevation changed lead to 0.05 dB. This discrepancy was not resolved.

The parts of the survey made at the lower elevations were normalized to that at 52°.8 elevation. Assuming that the ground radiation and atmospheric emission were functions of elevation only, their contributions could be removed by calibrating the survey against a horn measurement. Howell & Shakeshaft (1966, 1967) had measured the brightness temperature at their zenith ($\delta=52°$) for $\alpha=11^{\text{h}}$ and 13^{h} at 610 and 1407 MHz. Scaled horns having a beamwidth of 15° were used. The interpolated brightness temperature at 820 MHz is 6.1 ± 0.6 K.

The absolute zero level was thus ±0.6 K and the error in the temperature scale was 6 per cent. The main contribution to the latter is the error in the full-beam solid angle. The use of the horn measurements for setting the zero level implicitly assumes that the zenithal extinction was 0.028 dB. If it were, in fact, 0.05 dB the atmospheric emission would be increased by 2.2 K and the brightness temperatures in the survey should all be decreased by 2.2 K. Fig. 1(d) shows the 820-MHz map of the Northern Hemisphere.

2.6 1420 MHz

A survey of the Northern Hemisphere at a frequency of 1420 MHz was performed with the Stockert 25-m telescope of Bonn University. It has been published in two parts. Part 1 (Reich 1982) covers the declination range $19°<\delta<90°$ while part 2 (Reich & Reich 1986) is for $-19°<\delta<19°$. At the time of writing we have the digitized data for part 1 but not for part 2. The spectral index maps derived from this survey in Section 3 therefore cover only the region with $\delta>19°$ although some indication is given of how the spectral index varies down to $\delta=-19°$. Measurements were of the total intensity.

In a similar manner to the 820-MHz survey, scans were made in azimuth at fixed elevation to keep the atmospheric contribution constant. The elevations were 50°.6 (that of the North Celestial Pole), 40° and 20° and the scan rates were 10°, 5° and 5° min^{-1}, respectively. Part 1 of the survey was concerned solely with scans at the highest elevation. Unlike the 820-MHz survey, scans were

made alternately in directions of increasing and decreasing azimuth. In this way a network of crossing points was built up and a minimization technique similar to that for the 'nodding scans' was used to set a consistent base level. The sky was fully sampled.

The full-beam pattern of the antenna out to 3°.5 was determined from scans across Cas A. The antenna signal was calibrated continuously against a noise diode. This in turn was checked regularly by measuring strong 3C sources. This internal calibration gave temperature-scale error of ±5 per cent. This temperature scale agrees with that obtained from comparison with the drift scan at $\delta=40°$ made by Webster (1974) with a 15° beam horn at 1407 MHz. As the contribution of the ground radiation at 40° elevation was found to be <0.1 K it was concluded that the contribution to part 1 of the survey was negligible. The constant atmospheric contribution to part 1 of the survey was removed and the absolute zero level was set by comparison with the absolutely calibrated horn measurements at 1407 MHz and $\delta=52°$ (Howell & Shakeshaft 1966) and at 1435 MHz and $\delta=22°$ (Pelyushenko & Stankevich 1969). The error in the absolute zero level was ±0.5 K. Fig. 1e shows the 1420-MHz map for $\delta>19°$ corresponding to part 1 of the survey.

In part 2 of the survey the lower elevation meant that the observations had to be corrected for ground radiation. The range of azimuths scanned was such that there was sufficient overlap in declination so that the data taken at an elevation of 40° could be normalized to the, now, absolutely calibrated part 1 of the survey and then the 20° elevation data could be normalized to that at 40°. As there has been no absolute horn measurement in the $\delta<20°$ region, a gradient in the absolute base level could not be ruled out.

2.7 SUMMARY

The characteristics of the surveys are summarized in Table 1. The 'extragalactic background' and the 'base level correction' are discussed in the next section.

Table 1. Characteristics of radio continuum surveys

Frequency	HPBW	Scale error	Base level error	Extragalactic background	Base level correction
MHz	Deg.	per cent	K	K	K
38	7.5	5	300	2185	—
178	0.22×5	10	15	33.9	+27.5
408	0.85	10	3	5.89	—
820	1.2	6	0.6	3.17	−0.97
1420	0.6	5	0.5	2.80	−0.13

3 The spectral index distribution

As we wish to determine the spectral index of the Galactic emission only, the extragalactic emission must first be subtracted. This is made up of two isotropic components, the cosmic background radiation, or 'relict' radiation, and the sum of unresolved extragalactic sources.

3.1 THE COSMIC BACKGROUND RADIATION

In a review article, Weiss (1980) lists the measurements of the temperature of the cosmic background radiation using conventional microwave techniques in the Rayleigh–Jeans part of the spectrum. We eliminate those performed at frequencies below 4 GHz as they contain an appreciable contribution from the Galactic emission that can only be subtracted when its spectral index is assumed. The weighted mean of the 12 remaining determinations is 2.726±0.083 K. We adopt a value of 2.7 K.

3.2 EXTRAGALACTIC RADIO SOURCES

Bridle (1967) used observations with scaled antennae at frequencies between 13.15 and 81.5 MHz to obtain a value for an isotropic component. He used the method of T–T plots (see Section 4), which required that the spectral index of the isotropic emission first be specified. Using β=2.75, his estimate of the mean index of radio galaxies, he obtained a brightness temperature of the isotropic background equivalent to 48±11 K at 150 MHz.

There are two objections that could be made to this value. First, the method adopted to separate the isotropic background is based on the assumption that the anisotropic Galactic emission has a uniform spectral index. Secondly, the background may include Galactic emission that is coming from regions of the halo sufficiently far from the Sun that it is so nearly isotropic as to be indistinguishable from the extragalactic background.

An alternative approach is to integrate the source count data. For instance, Willis *et al.* (1977) give analytical expressions which fit the Westerbork counts at 610 and 1415 MHz. The integrated brightness temperature for all sources above the limiting flux densities of the surveys are 0.60 and 0.059 K, respectively. These give a spectral index β=2.78 and an extrapolated value of 30 K at 150 MHz. At the limiting flux density, 6 mJy, of the 610-MHz survey, there is a strong convergence of the counts and, if this is extrapolated to all sources of lower flux density, the brightness temperature at 150 MHz is increased only marginally to 32 K.

Fortunately the extragalactic background from unresolved sources make no more than a minor contribution to the total brightness temperature at any frequency so that the precise value is not of crucial importance. We have adopted a value of 50 K at 150 MHz and a spectral index of 2.75. This is probably an upper bound on the contribution from extragalactic sources.

3.3 BASE-LEVEL ERRORS

After subtraction of the extragalactic contribution, the brightness temperature spectral index $\beta(f_1/f_2)$ of the Galactic radiation, T_G, between frequencies f_1 and f_2 can be calculated. If it is assumed that the spectrum is a power law between these two frequencies, $\beta(f_1/f_2)=\log[T_G(f_1)/T_G(f_2)]/\log(f_2/f_1)$. The data with the higher angular resolution must first be convolved so that the angular resolutions are the same at both frequencies. For instance, to obtain β(408/1420) the 1420-MHz data was convolved to the 0°.85 angular resolution of the 408-MHz data.

When the distribution of β(408/1420) over the Northern Hemisphere was displayed on a stereographic projection with a grey-scale representation it was apparent that there were radial striations along the scanning directions of the 408-MHz survey and curved striations lying along the scanning directions of the 1420-MHz survey. This was due to small baseline errors that remained after the application of the minimization technique to the crossing points of the upward and downward scans. For the 408-MHz data the residual errors are <1.5 K and are barely apparent on the published brightness temperature maps. When the ratio of brightness temperatures at two different frequencies is calculated, however, the effect of these residual errors is enhanced. (See for example fig. 5 of Kallas *et al.* 1983). The same effect is seen on spectral index maps involving the 820-MHz survey. It should be possible to remove the effect by smoothing the data perpendicular to the scanning direction but, because the scanning directions differ from one survey to the next, one would not then be able to compare like with like. We adopted the simpler procedure of convolving both sets of data to a common resolution, low enough that the residual baseline errors are averaged sufficiently for the effect on the grey-scale representation to disappear. By trial this was found to occur when the resolution was reduced to 4°. The surveys at 408, 820 and 1420 MHz were therefore convolved to a resolution of 4° before spectral indices were calculated. These convolutions are shown in Fig. 1(c), (d) & (e). It was not necessary to convolve the 38-MHz data to a lower resolution than the actual one of 7°.5.

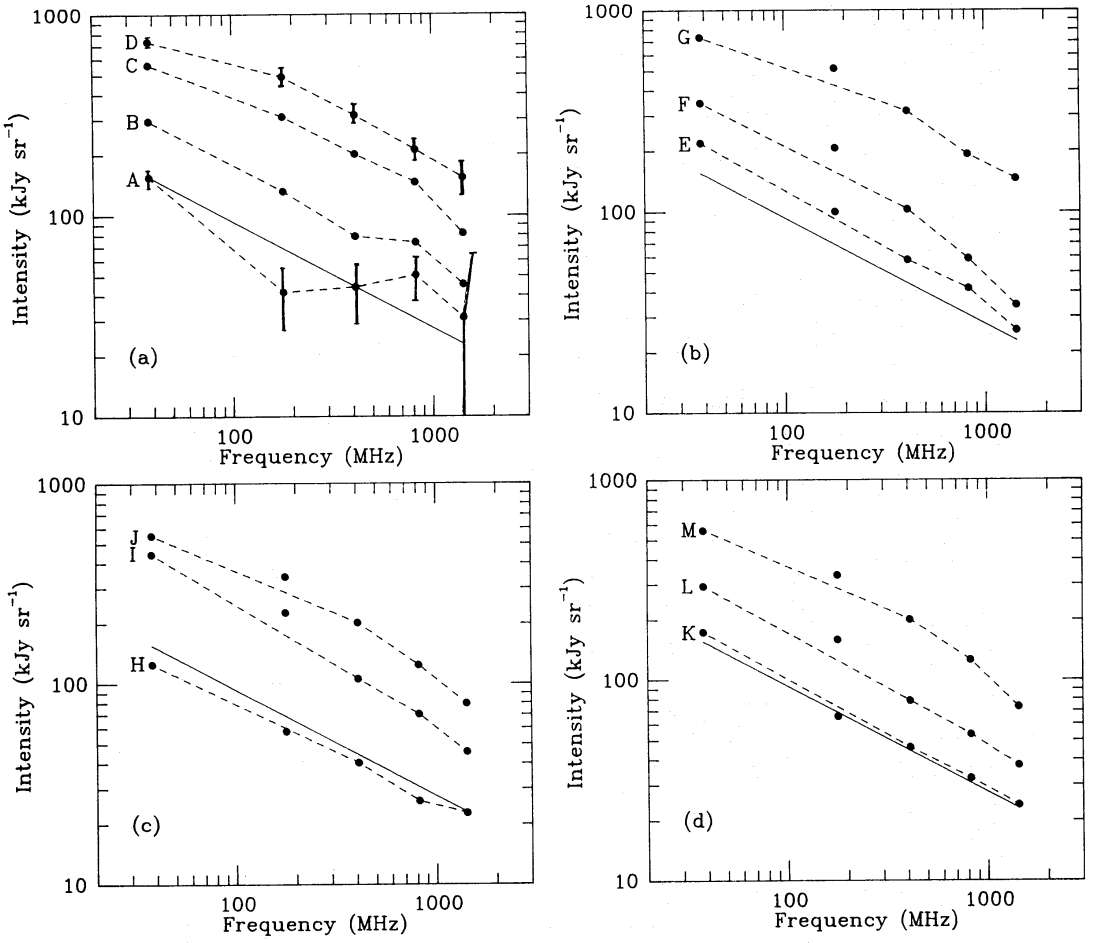

Figure 2. Intensities of Galactic emission for representative points. (a) Observed intensities. A: average over the 'sky minimum' region as defined in Section 3.3. B: intensities at α=0°, δ=20°. C: intensities at α=90°, δ=20°. D: intensities at α=320°, δ=55°. The solid line on each plot shows the adopted intensities for the 'sky minimum' region. (b) Corrected intensities for δ=55°. E: α=150°. F: α=270°. G: α=320°. (c) Corrected intensities for δ=35°. H: α=140°. I: α=270°. J: α=80°. (d) Corrected intensities for δ=20°. K: α=140°. L: α=0°. M: α=90°.

In Fig. 2(a) the intensity of Galactic emission at the five available frequencies is plotted for some representative directions on the sky. The observed brightness temperatures, after subtraction of the extragalactic components, have been converted to intensities using expression 2.1. The dashed lines serve simply to connect the intensities for a particular direction. The points marked A refer to the mean intensity over the region of sky with the lowest brightness temperature ($20°<\delta<50°$ and $130°<\alpha<150°$). The error bars shown on points A and D were obtained by combining the base level and scale error of Table 1. For the 'sky minimum' intensities the relative errors are large and, in particular, the spectral index beyond 820 MHz is unknown. The reason is that the base-level error of ±0.5 K at 1420 MHz, although not especially large in comparison with the total brightness temperature, represents 100 per cent of the residual Galactic emission. One must conclude that the form of the spectrum of the Galactic emission from the 'sky minimum' direction is only weakly constrained by the surveys. The base-level errors, as they stand, would appear to imply quite large uncertainties in the spectral indices even in regions of high intensity. The problem is to fix the zero levels of the surveys in absolute terms.

A traditional approach, that adopted by Kallas *et al.* (1983), is to construct a 'T–T' plot. In such a plot, brightness temperatures at one frequency are plotted against those at a second frequency

over a chosen area of the sky. A straight line is fitted to the points. The slope leads to the spectral index between the two frequencies while the intercepts fix the base level at one frequency relative to that at the second. The problem is that the requirements that the spectral index be uniform over the chosen area, but that the intensities show a large enough variation to give an accurate straight-line fit, may be mutually exclusive. Even if there are genuine variations in the spectral index it is always possible to perform a least-squares fit to the T–T plot, but the meaning of the base-level values so obtained is obscure. We have chosen an alternative approach. The spectral index of the 'sky minimum' is that most sensitive to changes in the base level. One might expect it to be constant or monotonically increasing with frequency. We take the simple assumption that it is constant at a value given by the surveys at 38 and 408 MHz, as they have the smallest fractional errors, and adjust the base levels of the others to fall in line. The adopted spectrum of the 'sky

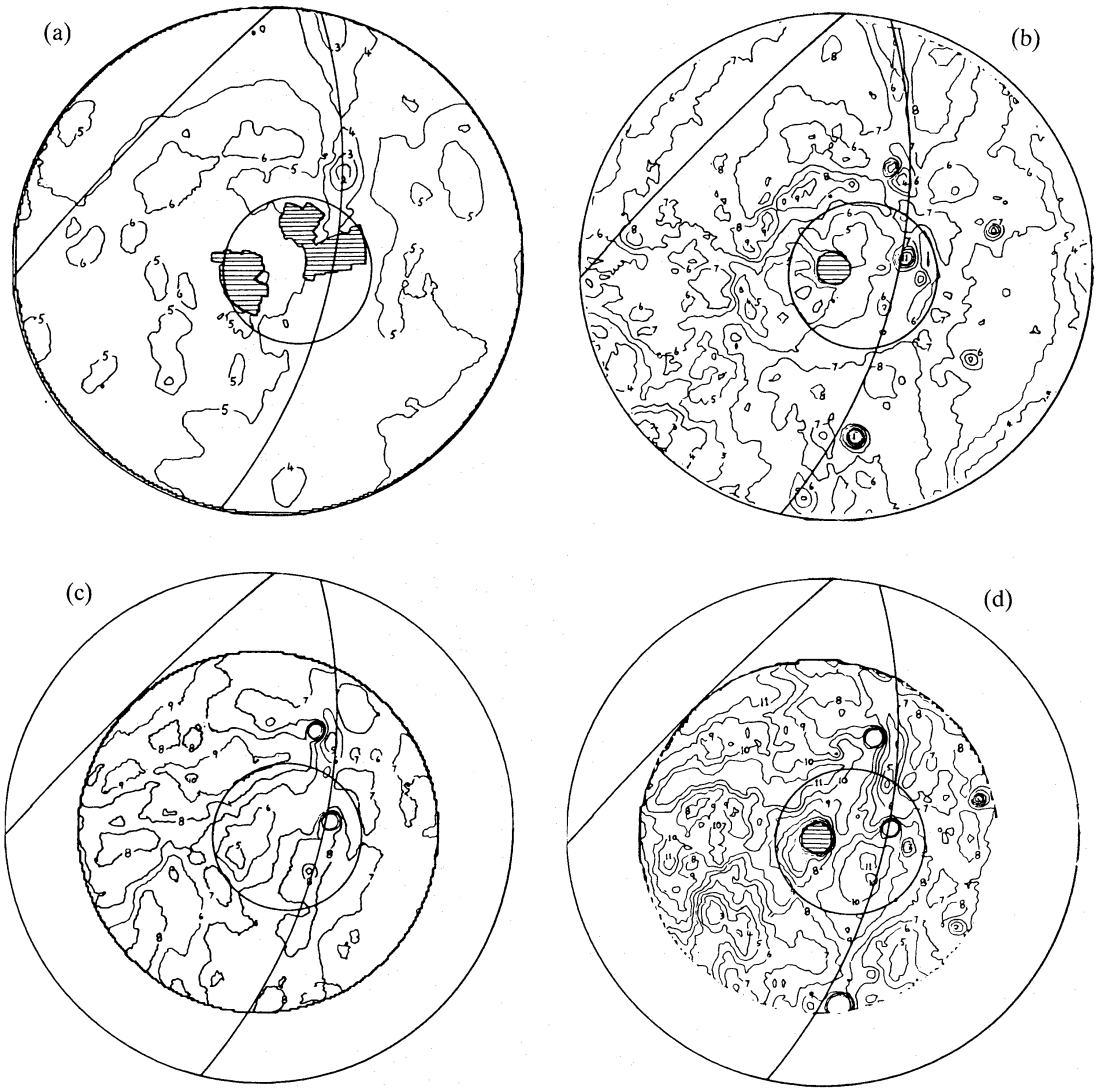

Figure 3. Contour maps of brightness temperature spectral index over the North Celestial Hemisphere. The stereographic projection and orientation of the plots is the same as for Fig. 1. The Galactic equator $b=0°$, and the ridge lines of loops I and III as in Fig. 1(d) & (e), are shown. Contour labels 3, 4, ..., 9, 10 correspond to spectral indices $\beta=2.3, 2.4, \ldots, 2.9, 3.0$. (a) The spectral index between 38 and 408 MHz. The 408-MHz survey was convolved to the 7°.5 beamwidth of the 38-MHz survey. (b) The spectral index between 408 and 820 MHz. Here and in Fig. 2(c) & (d), both surveys were convolved to a beamwidth of 4°. (c) The spectral index between 408 and 1420 MHz. (d) The spectral index between 820 and 1420 MHz.

minimum' is indicated by the solid line in Fig. 2(a) and the 'corrections', which are to be added to all the brightness temperatures at the given frequency, are listed in the last column of Table 1. In the event the corrections are similar to, and in the same sense as, those obtained by Kallas *et al.* although they take the 1420-MHz temperatures as the datum and correct the 820- and 408-MHz temperatures.

The adjustment to the 178-MHz data is about twice as large as the quoted error and exacerbates an existing anomaly in the regions of higher intensity. The effect is as if the correction for the relatively large sidelobes of the antenna had been overestimated. There is independent evidence for this from the comparison with drift scan observations (Section 4.1). We reluctantly conclude that the 178-MHz survey cannot be relied upon for determining a spectral index distribution.

After the corrections to the base levels had been made and the extragalactic contributions had been subtracted the spectral index distributions of Fig. 3 were obtained. To make the rather complex form of the variations clearer, an alternative grey-scale representation is given in Fig. 4. The distributions show contrasting behaviour above and below 408 MHz. At the lower frequencies the variation across the sky is small. The index near to the Galactic plane and along the ridges of the loops is close to 2.5 (corresponding to an E^{-2} electron spectrum) and is marginally smaller than away from the plane and between the loops. Above 408 MHz the spectrum becomes progressively steeper on the outside of the loops and exceeds 3.0 between loops I and III. The specific values of the spectral index in this higher frequency region, but not their general behaviour, depend on our assumption that the index of the 'sky minimum' region is constant. If this in fact increases at high frequencies, the index will be even steeper on the outside of the loops. There is evidence, discussed in the next section, however, that the base-level values we have used are close to the actual ones.

4 Comparison with earlier work

4.1 LOW ANGULAR RESOLUTION SCANS

Low angular resolution drift scans along declinations 20°, 40° and 60° were made by Turtle *et al.* (1962) at 26, 38 and 178 MHz. Scaled corner reflector arrays having beamwidths 15°×44° were used. Purton (1966) made corrections to the temperature scale at 26 and 38 MHz and added a drift scan at 81 MHz. Scans using a 7.5-m paraboloid at 404 MHz were also made and convolved to the lower resolution of the corner reflectors. T–T plots were constructed for each pair of scans in RA at constant declination. If the spectral index of the anisotropic (Galactic) contribution to the total brightness temperature were independent of RA the T–T plot would be a straight line from whose slope the spectral index could be calculated. The advantage is that no assumptions need be made concerning the spectral index of any isotropic (extragalactic) contribution and any constant base-level errors do not affect the derived spectral index. In the event the T–T plots are not single straight lines. Each drift scan has a minimum between 9^h and 10^h RA. Each T–T plot can be fitted approximately by two straight lines intersecting at the point representing the minima at the two frequencies. If temperatures for the higher of the two frequencies are plotted along the abscissa, the fitted straight line for RAs preceding 10^h has a smaller slope than that for RAs following 10^h. Turtle *et al.* define a region I as having $3^h<\mathrm{RA}<10^h$ and thus covering the broad Galactic disc in the region of the anticentre and extending to $b=50°$ (see Fig. 1a). Region II has $10^h<\mathrm{RA}<17^h$ and is referred to, by the authors, as the halo region. One should note, however, that even in the direction of the Galactic North Pole, about half of the total line-of-sight emission would be expected to be coming from the Galactic disc. Spectral indices deduced are $\beta(38/178)=2.36\pm0.04$ and $\beta(38/404)=2.55\pm0.03$ in region I and 2.47 ± 0.04 and 2.60 ± 0.02, respectively in region II. The $\beta(38/404)$ in region I is in agreement with our $\beta(38/408)$ values

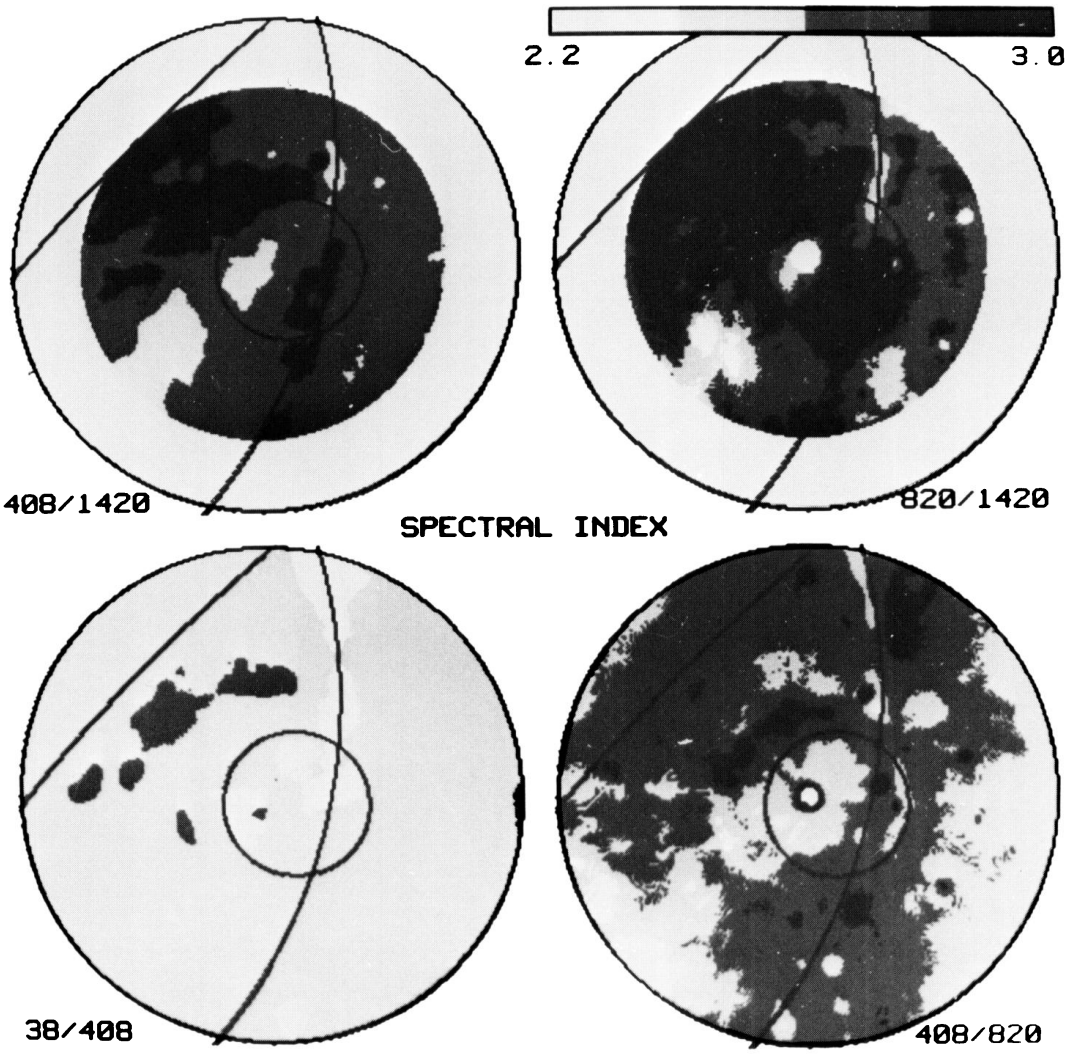

Figure 4. Grey-scale map of the brightness temperature spectral index over the North Celestial Hemisphere. The maps correspond to those of Fig. 3.

[*facing page* 318]

averaged over this region. The region II values agree too but the rather large variation in spectral index that we see, from the low index loop I to the higher index between loops I and III means that an overall average index is not particularly meaningful. One can say that above 178 MHz there is an indication from both regions that the spectrum is beginning to steepen. Howell (1970) extended these low-resolution scans to a measurement at 610 MHz and found $\beta(81.5/610)$ to be 2.58 ± 0.03 and 2.57 ± 0.03 in regions I and II, respectively.

Bridle (1967) performed higher angular resolution drift scans at 17.5 and 81.5 MHz using $2.5\lambda\times4\lambda$ dipole arrays. These had beamwidths of $17°\times12°$. He gives a contour map of $\beta(17.5/81.5)$ from the North Pole to declination $+16°$. This is similar to the present $\beta(38/408)$ distribution in that the highest index is in the region between loops I and III running from $b=15°$ to the Galactic North Pole, while the lowest is along the plane. His is the index of the total brightness temperature. When our assumed extragalactic component is subtracted, the resultant index is smaller by 0.1 than our values. The difference barely exceeds the quoted uncertainty but also indicates progressive steepening towards 408 MHz. Again, in order to obtain spectral information on the anisotropic component alone, T–T plots were made. With the higher resolution, regions I and II were made smaller than those given above, in order to avoid the Galactic plane and loop I, and were redefined as $140°<l<220°$, $15°<b<50°$ for region I and $b>70°$ for all l plus $50°<b<70°$ for $50°<l<90°$ plus $30°<b<50°$ for $70°<l<90°$ region II. Region I was referred to as the 'local spiral arm' while region II was called the 'interarm'. In region I, most of the emission will be from the Orion spur, which appears to be a branch of the main spiral structure lying just outside the Sun's position in the Galaxy, but some will come from the halo region above the Perseus arm. Region II would appear to contain emission from the halo region lying above the continuation of the Orion spur towards the direction in which it joins the Perseus arm. If the Sun does lie in the interarm, that part of Region II near to the Galactic North Pole does indeed contain interarm emission although about half of the total might arise in the halo. The $\beta(17.5/81.5)$ indices are 2.38 ± 0.04 and 2.45 ± 0.04 respectively. Bridle also finds that the North Polar Spur has a lower spectral index than its surroundings.

Sironi (1974) completed drift scans with identical dipole arrays, scaled with wavelength at 151.5 and 408 MHz. We have simulated the scans using the theoretical beam shape of the array and the survey data at 178 and 408 MHz (scaling the former by an assumed spectral index of 2.6 to allow for the small difference in frequency between the survey and the drift scan). As the drift scan observations were made with respect to an arbitrary base level, we normalized the observations and simulations at the lowest temperature on each scan. Regarding the 151.5-MHz drift scans, there is good agreement for declinations 40° and 52°. For declinations 16°, 30°, with normalization having been made at 200 K, the simulations tend to be 10 per cent higher at 500 K. This discrepancy would be accounted for if the Turtle & Baldwin data had indeed been overcorrected for sidelobe effects as suggested in Section 3.

The 408-MHz drift scan observations and simulations also showed some systematic differences in the 6^h to 10^h range of RA. After normalization near 20 K, they all show the observations to be about 15 per cent higher than the simulations at 35 K. In this case it seems clear that the drift-scan data are at fault because, in contrast, excellent agreement is found between Webster's (1974) drift scans using a horn antenna and the simulation obtained by applying the theoretical beam of the horn to the 408-MHz survey data (Fig. 5). Sironi gives $\beta(81.5/408)=2.41\pm0.04$ for Bridle's region I. If instead one uses the simulated drift-scan data this index for region I is increased to 2.50 in agreement with Fig. 3(a). The observations and simulations agree in the 10^h to 18^h range and the value $\beta(81.5/408)=2.59\pm0.11$ also agrees with Fig. 3(a).

Webster (1974) performed drift scans using scaled horn antennae with HPBW of 15° at 408, 610 and 1407 MHz. Again the regions I and II of Bridle were picked out (refered to as Zones A and B in this publication). For region I $\beta(408/610)$ is 2.92 ± 0.07 while for region II it is 2.75 ± 0.06. The

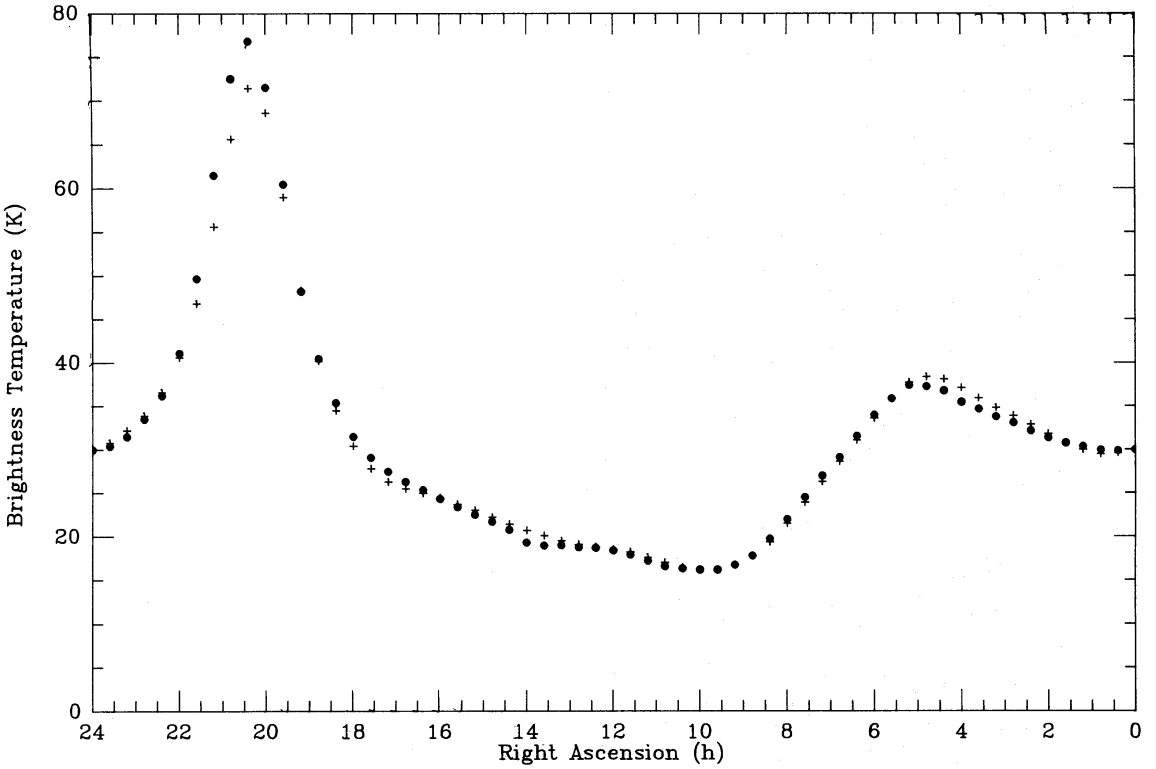

Figure 5. Comparison of actual and simulated 408-MHz drift scans at $\delta = 40°$. Filled circles: observations by Webster (1974). Crosses: simulated drift scan obtained by convolving the brightness temperatures of the Haslam *et al.* (1982) survey by the theoretical beam of the horn antenna. The observations are normalized to the simulation at the lowest temperature.

indices differ in the opposite sense from that which would be expected from the $\beta(408/820)$ distribution in Fig. 3(c) and also from the lower frequency results. Webster concluded, however, that the difference between the two regions was barely significant and quoted a mean value at high northern latitudes of 2.80 ± 0.05. At 1407 MHz the scans were made only for declinations 0°, 16° and 40° (the latter omitting the RA range 2^h to 14^h). The spectral indices for the two regions and three declinations show rather large variations and errors. This is a result of the T–T plots having poor fits to straight lines. The best estimate overall of $\beta(408/1407)$ is again 2.80 ± 0.05. When the T–T plots were examined in more detail a number of regions with anomalous spectral index were noted. The spectrum of the ridge of loop I is steeper than the general background while that within the ridge is flatter than the average. The same applies to loop III. For the scan at declination 40°, the T–T plots between all three pairs of frequencies show evidence of a spectrally steep feature between 14^h and 18^h. This corresponds exactly to the area of steepest spectral index on each of Fig. 3 (b), (c) & (d).

One can conclude that the earlier low-resolution work is in very good agreement with the higher-resolution spectral index distributions that are presented in Section 3 and this lends support to the procedure adopted there for fixing the base levels.

4.2 THE WORK OF BERKHUIJSEN (1971)

Berkhuijsen (1971), in a discussion of the results of her 820-MHz survey, considered the spectral index of some features in the Northern Hemisphere for which partial surveys at other frequencies with beam sizes of about 1° were then available. The survey by Haslam, Large & Quigley (1964) at

240 MHz was used to produce T–T plots across the ridge of loop I (specifically along lines of constant Galactic latitude from 17° to 43° for longitudes from 15° to 45°). The best-fitting straight lines to the plots gave an overall mean $\beta(240/820)=2.66\pm0.02$. The fact that the plots are closed loops rather than straight lines indicates, however, that there is a variation of spectral index across the ridge. It was deduced that the spectral index inside the ridge is lower by about 0.1 than outside the ridge. Similarly the spectral index across loop III was found to be 2.55 ± 0.05. The values are in good agreement with the $\beta(38/408)$ distribution of Fig. 3(a) if one assumes that $\beta(240/820)$ is greater than $\beta(38/240)$ by about 0.1.

4.3 THE GALACTIC HALO AS INFERRED FROM DRIFT SCANS

As mentioned in Section 4.1, the T–T plots of the Northern Hemisphere do not take the form of single straight lines. Rather there is a line of lesser slope for RA preceding the direction of minimum intensity at about 10^h, and a line of greater slope for later values of RA. Webster (1975) pointed out that such 'loops' on the T–T plots would be the expected signature of a Galactic halo, having a minimum surface brightness in the general direction of the Galactic anticentre and a spectrum steeper than that of the disc. To quantify the signature he considered the area of the loop on each plot described by a point moving along the plot from $\alpha=6^h$ to $\alpha=18^h$ and then returning by a straight line to 6^h. (This range of RA restricts the plot to positive values of Galactic latitude. He went on to infer the parameters of the simplest halo model that would produce this signature, namely, a spherical halo of uniform emissivity and spectral index. The often quoted values obtained were a radius of 12.5 kpc and an emissivity at 80 MHz about 5 per cent of that of the disc.

Bulanov, Syrovatskii & Dogiel (1976) remarked that the assumption that the halo spectral index is uniform leads to a lower estimate of the halo emissivity than would be obtained from a more physically realistic model in which the spectral index increases with distance from the plane. Strong (1977) used a model in which electrons from sources near to the Galactic plane diffuse into an unbounded region while undergoing synchrotron and inverse Compton losses. He compared his predictions with the observed shape of the T–T loop as defined by the function

$$F(\alpha,\delta)=T(\alpha,\delta,f_1)(f_1/f_2)^{\beta_d}-T(\alpha,\delta,f_2)=F_h(\alpha,\delta)-F_e. \tag{4.1}$$

This function eliminates the contribution of the Galactic disc provided that it has a known, uniform, spectral index β_d. F_h is related to that part of the halo surface brightness at frequency f_2 that can be distinguished from the disc emission by virtue of its steeper spectrum, and F_e is an isotropic contribution from extragalactic radio sources. Graphs were plotted of the variation of F with α for various fixed values of δ derived from brightness temperatures at 17.5 and 81.5 MHz. They could be fitted by a combination of halo magnetic field strength, energy-loss rates and diffusion coefficient which lead to a halo component of the emissivity distribution about the Galactic plane having a full width at half maximum of about 6 kpc. The local halo emissivity just outside the disc is required to be about 10 to 20 per cent of the local disc value, the difference in emissivity being attributed to a lower magnetic field in the halo than in the disc.

Independently Webster (1978) used the same function in a model where the halo had a uniform emissivity and spectral index but was a spheroid whose axial ratio and size were free parameters. For the 17.5/91.5 MHz data a prolate spheroid with semi-axis in the Galacic plane, $A=12.2$ kpc and semi-major axis perpendicular to the plane, $B=17$ kpc was indicated, while for the 81.5/408 MHz data an oblate spheroid with $A=11$ kpc and $B=5$ kpc was required. Thus while both Strong and Webster have obtained fits to Bridle's 17.5- and 81.5-MHz drift scans, their fits correspond to very different geometries for the halo. Using Strong's value for F_e in Webster's approach gives a best fit for a spheroidal halo with $A=17$ kpc and $B=17.9$ kpc. It can be seen

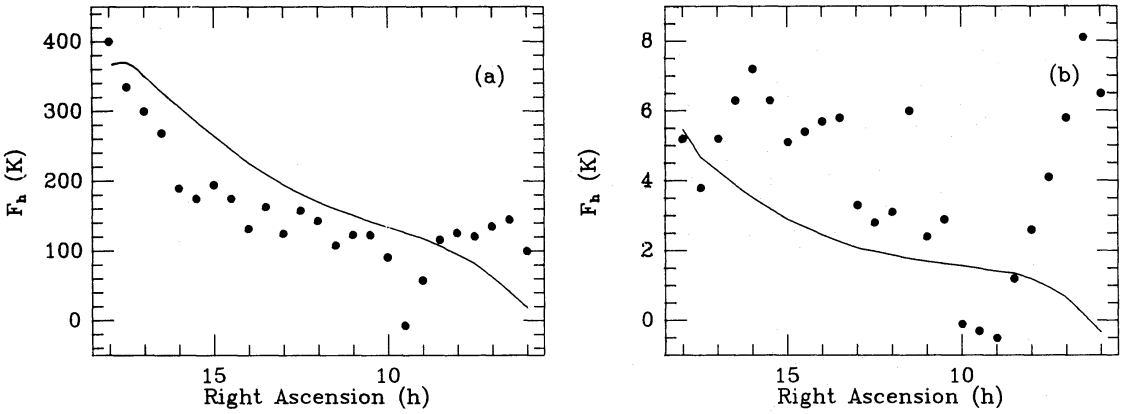

Figure 6. The function F_h, a measure of the surface brightness of the Galactic halo, evaluated (a) between 81.5 and 408 MHz and (b) between 408 and 1420 MHz for $\delta=35°$. The solid line is the prediction of the model by Strong (1977) which he fitted between 17.5 and 81.5 MHz.

therefore that the values of the parameters that describe the halo that are deduced from $F(\alpha, \delta)$ are very model-dependent.

We have extended these methods to the surveys at 408 and 1420 MHz. Fig. 6 shows that Strong's model provides a reasonably good fit to the parameter F_h derived from Bridle's (1967) drift-scan observations at 81.5 MHz and Sironi's (1974) observations at 408 MHz, both in terms of shape and absolute value. Also shown is the model prediction for the parameter F_h between 408 and 1420 MHz together with the observations. It is clear that in this case the model does not fit the observations at all well. It should be noted that when the predictions are compared with the observations it is the shape of the curve that is important. Errors in the zero levels of the surveys or in estimates of the extragalactic contribution simply produce a constant offset in the curves.

The main reason that neither Webster's model nor Strong's model fits the observations between 408 and 1420 MHz is that their halos, having spectral indices greater by 0.3 or 0.4 than that of the disc, are weak at these high frequencies and lead to a small variation of F_h with RA. The much larger observed variation of F then has to be ascribed to the effects of the emission associated with loops I and III even though, at $\delta=35°$ for instance, the emission is coming from considerable angular distances from these loops. If this is the case, it must cast doubt on the conclusions drawn at lower frequencies where it was assumed that drift scans that did not cross the ridge lines of the loops were free from contamination with emission associated with the loops.

5 Interpretation

We point out the following features of the spectral index maps of Fig. 2. The index $\beta(38/408)$ is lower along the Galactic plane than at high Galactic latitudes apart from the region around the ridge lines of loops I and III. An increase of spectral index with Galactic latitude is to be expected in the conventional picture where cosmic ray electrons are accelerated in the Galactic plane and lose energy by synchrotron radiation in propagating outwards through a Galactic halo. By contrast, however, above 408 MHz the following features are present. The spectral index in the vicinity of loops I and III is distinctly steeper than the spectrum of the background emission. The smallest values of β occur in the coldest parts of the sky. (Another very flat spectral region is that in the Cygnus region but the Cygnus complex is a known region of thermal emission.) There is a steep-spectrum region in the plane of the Galaxy between Galactic longitudes 115° and 165° which correlates well with the highly polarized 'fan' region of Wilkinson & Smith (1974) and the broad region of continuum emission about the Galactic plane. This feature has been discussed at length

by Kallas *et al.* (1983). The general picture appears to be that the emission associated with loops I and III and with the Galactic plane in the vicinity of loop III has a spectrum that steepens around 408 MHz while the background emission has a spectrum which, if it steepens at all, does so at a high frequency.

There is a general consensus that the loops are nearby, old supernova remnants (SNRs). The radio emission from the loops has been calculated by Spoelestra (1972) in terms of the van der Laan model in which there is compression of the interstellar cosmic ray electrons and magnetic field behind a cooling SNR shock front. Assuming an homogeneous interstellar medium, one can choose values for the parameters of the expanding shock which give sufficient compression to account for the observed surface brightness. If the electrons and magnetic field are merely compressed, however, the energy interval of the electrons producing the synchrotron emission is shifted towards smaller energies where observations show that any change of the spectral index of the electrons is in the sense of a decrease. The loops should therefore have flatter spectral indices than the surroundings at all frequencies. Spectral steepening by synchrotron losses would be significant within the estimated 10^5 yr lifetime of the SNR only if the magnetic field were increased by a factor >50 in the compression. This is a far larger field than is required to account for the surface brightness of the loops. Measurements of the Zeeman splitting of the 21-cm H I line within loop I and in the H I feature adjacent to the North Polar Spur ridge line (Troland & Heiles 1982) give upper limits to the line-of-sight component of the magnetic field of about 5 μG. The indication is that there is no more than a modest compression of the ambient magnetic field.

Blandford & Cowie (1982) have modified the van der Laan theory taking into account the effects of the multicomponent interstellar medium (McKee & Ostriker 1977). The largest fraction of space is occupied by the Galactic coronal plasma and the SNRs remain in their adiabatic phase throughout their radio-emitting lifetimes. Clouds enveloped by the shock front have shock waves driven into them. They propose that ambient interstellar cosmic rays with energies >25 MeV are accelerated by the first-order Fermi process in the shock fronts in the clouds. Additional enhancement of the synchrotron emissivity occurs if the shock is radiative and the compression ratio rises to a value limited only by the pressure of the embedded magnetic field. For SNR of radii 10 to 20 pc the shocks in the cold cloud component become radiative. The compression is such that it contributes a larger factor than does the acceleration to the enhancement of the overall emissivity of the SNR. For SNR with radii >30 pc the clouds constituting the warm phase of the interstellar medium would develop radiative shocks. For an SNR of radius 100 pc the compression factor after cooling is only slightly greater than the adiabatic value of 4 and the enhancement of emissivity is largely due to the shock-front acceleration. Blandford & Cowie show that a surface brightness compatible with observations of the large loops would be produced. The acceleration is due to strong shocks and the cosmic ray electron energy spectrum would be of the form E^{-2}. The radio spectrum would be flatter, rather than steeper than that of its surroundings. Also it is not apparent that such a clearly defined shell structure as that which is observed along the North Polar Spur would result.

Soft X-ray emission from loop I supports its identification as an SNR and gives information on the density and temperature of the gas in its shock front. No enhancement in the soft X-ray emission along the ridge of loop III has been observed. The maps by McCammon *et al.* (1983) cover the whole of loop III and most of loop I. From these we obtain upper limits to the emission from loop III which give some constraints on the possible models. After subtracting off an uncertain background rate, we estimate that in the *M*-band (0.45–1 KeV) the count rate from the ridge of loop III is at least three times smaller than that in the bright part of the ridge of loop I. The upper limit to the count rate from loop III in the *C*-band (0.15–0.28 keV) is approximately the same as in the *M*-band.

For the case of loop I there is information on its distance, and thus on the radius of its assumed

spherical shell, from stellar polarization studies. Berkhuijsen (1973) gives a radius of 115±68 pc with its centre at 130±75 pc. We note that the quoted value of 130±30 pc for the radius of loop III is based solely upon the fit of the van der Laan model due to Spoelstra. We have already questioned the application of the van der Laan model to this loop but in any case the fit is subjective, and if other of the free parameters are allowed to vary we find that a larger range of radii can be accommodated. Nevertheless we start by assuming a radius of 100 pc.

We consider the shock front in the coronal phase of the interstellar medium using the values of density and temperature from McKee & Ostriker (1977), namely $n_0=3.5\times10^{-3}$ atom cm^{-3} and $T_0=4.5\times10^5$ K. At large radii the effect of the finite pressure, P_0, of the interstellar medium on the SNR expansion begins to show and the treatment by Hayakawa *et al.* (1979), which takes this into account, was used. The shock-front velocity at radius R is given by

$$V=\{(P_0/3\varrho_0)[1+4K(1+x)]\}^{0,5}, \tag{5.1}$$

where $K\simeq1.1$ and $x=E_0/(2\pi P_0 r^3)$. The density jump at the shock front is

$$y=[4K(x+1)+1]/[K(x+1)+4] \tag{5.2}$$

and the temperature jump is $[4y-1]/[y(4-y)]$. If we take the initial energy of the explosion, E_0, to be 10^{51} erg and R to be 100 pc then the temperature of the shock is 2×10^6 K. From the M-band emission of loop I, Hayakawa *et al.* derive a temperature of 3.3×10^6 K. From the upper limit to the M-band emission of loop III we deduce an upper limit to the temperature of its shock of 1.6×10^6 K, taking the emission measures of the two loops to be the same. To be compatible with this a slightly larger radius of 110 pc is needed. This gives $V=326$ km s^{-1} and a density jump $y=3.0$. If the enhancement of emissivity were due to compression, a maximum surface brightness of only 3.5 K at 408 MHz would be obtained. Some additional acceleration of electrons is needed.

At an earlier stage of the present study of the spectral index distribution when only the information on $\beta(408/1420)$ was available, Dogiel, Mayer & Osborne (1983) considered that a model of diffusive shock acceleration from the coronal phase of the interstellar medium might give a possible explanation of the steep index associated with loop III. Although this model can now be ruled out by the lower-frequency observations, it is worth repeating some of the arguments here. A change of the accelerated particle spectrum at the shock front is possible only if the ambient spectrum is steeper than the spectrum created by the shock-wave acceleration acting on initially monoenergetic particles. It is necessary first that there is efficient acceleration of particles having smaller energies than the radio-emitting electrons, but with a steeper spectrum than that created by the shock-wave acceleration. An upper limit to the intensity of the accelerated electrons corresponds to all of the electrons in the volume being accelerated, including thermal electrons. Bulanov & Dogiel (1980) showed that this non-injective acceleration can be realized if the acceleration time, $t_A(p)$, is less, for all momenta, than the minimal ionization loss time, which is about 10^{10} s. The acceleration time $t_A\simeq D/V^2$, where D is the diffusion coefficient of the cosmic ray particles near the shock front. With V as estimated above, $D<10^{25}$ cm^2 s^{-1} would be required for non-injective acceleration. Analysis of the composition of the nuclear component of the cosmic rays gives an average Galactic diffusion coefficient in the region of 10^{28} cm^2 s^{-1}, so that enhanced scattering in the vicinity of the shock front compared with that which controls escape from the Galaxy would be necessary. Dogiel *et al.* went on to show that, with the values of R and V appropriate to the loops and a value of D small enough for non-injective acceleration, the steepening of the spectrum due to the curvature of the shock front would be very small. The energy spectrum of the accelerated particles has an index $(y+2)/(y-1)$. For a density jump $y=3$, this has a value of 2.5, giving a brightness temperature spectral index of 2.75. From the predicted radial dependence of the electron intensity the distribution of surface

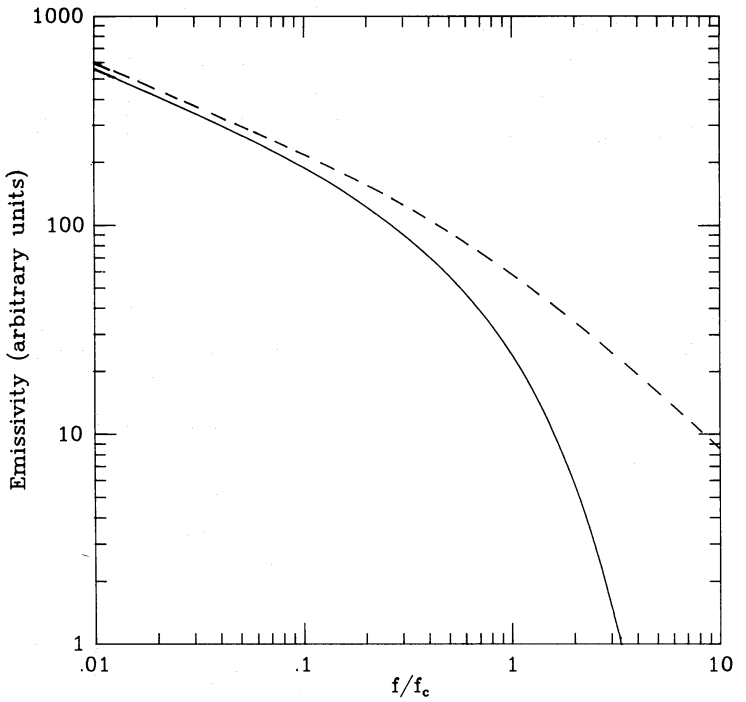

Figure 7. The form of the synchrotron spectrum due to an electron energy spectrum that is a power law of the form $E^{-1,8}$ for $E<E_0$ and (a) is truncated above E_0 (solid line) or (b) steepens abruptly to $E^{-2.8}$ above E_0. The frequency, f, is given in terms of the critical frequency f_0 of an electron with energy E_0. ($f_0=16\,BE_0^2$ MHz where B is in μG and E_0 is in GeV.)

brightness was calculated and found to have a peak value of about 50 K at 408 MHz consistent with the observations.

A firm prediction of the non-injective acceleration model is that the synchrotron spectrum should continue with the same steep spectral index down to the lowest frequencies. The observations discussed here show that this is not the case below 408 MHz. The flat synchrotron spectrum at these frequencies is consistent with the electron spectrum expected from a diffuse acceleration in a strong shock but the electron spectrum steepens at higher energies. It is important to realize that the synchrotron process gives a wide range of frequencies emitted by electrons of a given energy and that a power-law energy spectrum with a sharp increase in slope at a given energy results in a rather gradually steepening synchrotron spectrum. Fig. 7 shows the form of the synchrotron spectrum from an electron spectrum whose spectral index increases by unity at a given energy E_0. The observed synchrotron spectrum in the region of the loops appears to steepen more rapidly than this. (It should be remembered that the spectra in Fig. 2 relate to the total intensities summed over the line-of-sight. It is apparent that if these were to be separated into foreground and background components the former would exhibit a more drastic steepening. The exact form of the steepening is difficult to determine. We have, for instance, been able to obtain a picture of the 'local' emission at 408 MHz by subtracting off the large-scale Galactic emission predicted by the model of Phillipps *et al.* (1981) but, in order to obtain the precise form of the spectral index of the local emission, one would need a frequency-dependent model of the large-scale Galactic emission.) Also shown in Fig. 7 is the limiting case of steepening corresponding to the truncation of the electron spectrum at E_0. For a conventional value of the magnetic field strength of 3μG, the truncation energy, E_0, is between 5 and 10 GeV. The truncated spectrum would result if the acceleration time for the electrons, which is $\simeq D/V^2$, exceeded the age of the supernova remnants ($\simeq 10^5$ yr). One would need D to be increasing with

energy, reaching at E_0 about $10^{27}\,\mathrm{cm^2\,s^{-1}}$. This is still smaller than that due to the general interstellar turbulence, as deduced from a study of the composition of the nuclear component of cosmic rays, but not by more than an order of magnitude. The characteristic diffusion length of particles ahead of the shock, D/V, would be of the order of 10 pc and the effect of curvature of the shock front could also be of some importance.

6 Conclusions

It is suggested that the variation of the spectral index of the radio continuum emission over the Northern Hemisphere is mainly due to the effects of loops I and III. A qualitative explanation of the steepening of the spectrum of emission apparently associated with these loops has been put forward in terms of diffusive shock acceleration. A truncation in the electron spectrum is required at between 5 and 10 GeV. This is a lower energy limit than is proposed by those who favour diffusive shock acceleration as the main mechanism producing the observed energy spectrum of cosmic ray nuclei. Higher limits require a diffusion coefficient that is substantially smaller than that which one infers from the escape length of cosmic rays from the Galaxy. The smallest possible diffusion coefficient is that for which the scattering mean free path is equal to the gyroradius of the cosmic ray particles, but even this is insufficient for acceleration to operate up to the observed break in the energy spectrum of cosmic ray nuclei at 10^6 GeV. The proposed truncation at 5 GeV does not contradict the finding of Bhat *et al.* (1985) that gamma ray emission from the region of loop I is evidence for acceleration of cosmic ray nuclei and electrons. The gamma rays are produced by cosmic rays of lower energy than this.

There are other large-diameter supernova remnants that show evidence of steepening in their spectra. From the catalogue of Clark & Caswell (1976) we have considered those with diameters >40 pc. There are 17 whose fluxes have been measured at three or more frequencies with the highest frequency >1 GHz. Of these, five show a steepening in the spectrum which is consistent with a truncation in the electron-energy spectrum. They are HB9, S147, the Cygnus Loop, G33.2−0.6 and G126.2+1.6.

There are no surveys above 1.4 GHz away from the Galactic plane, but current experiments to measure anisotropies in the microwave background radiation at frequencies above 5 GHz may allow one to check our prediction that the surface brightnesses of loops I and III should be very low.

The Southern Hemisphere appears to be mainly free of the effects of such loops, so that southern surveys should give information on the spectral index of the larger-scale Galactic emission. A survey by the Instituto Argentino de Radioastronomia is under way and this will eventually lead to an all-sky map at 1420 MHz.

Acknowledgments

We are greatly indebted to Drs C. G. T. Haslam and W. Reich for providing their data in digitized form and for many illuminating discussions. We thank Dr J. Baldwin for providing the 178-MHz data. MLP acknowledges SERC for his Research Studentship.

References

Berkhuijsen, E. M., 1971. *Astr. Astrophys.*, **14,** 359.
Berkhuijsen, E. M., 1972. *Astr. Astrophys. Suppl. Ser.*, **5,** 263.
Berkhuijsen, E. M., 1973. *Astr. Astrophys.*, **24,** 143.
Berkhuijsen, E. M., Haslam, C. G. T. & Salter, C. J., 1971. *Astr Astrophys.*, **14,** 252.
Bhat, C. L., Issa, M. R., Mayer, C. J. & Wolfendale, A. W., 1985. *Nature,* **314,** 515.

Blandford, R. D. & Cowie, L. L., 1982. *Astrophys. J.,* **260,** 625.
Bridle, A. H., 1967. *Mon. Not. R. astr. Soc.,* **136,** 219.
Bulanov, S. V. & Dogiel, V. A., 1980. *Soviet Astr. Lett.,* **5,** 228.
Bulanov, S. V., Syrovatskii, S. I. & Dogiel, V. A., 1976. *Astrophys. Space Sci.,* **44,** 255.
Clark, D. H. & Caswell, J. L., 1976. *Mon. Not. R. astr. Soc.,* **174,** 267.
Dogiel, V. A., Mayer, C. J. & Osborne, J. L., 1983. *Proc. 18th ICRC, Bangalore TIFR, Bombay,* **9,** 231.
Haslam, C. G. T., Large, M. I. & Quigley, M. J. S., 1964. *Mon. Not. R. astr. Soc.,* **127,** 273.
Haslam, C. G. T., Quigley, M. J. S. & Salter, C. J., 1970. *Mon. Not. R. astr. Soc.,* **147,** 405.
Haslam, C. G. T., Salter, C. J., Stoffel, H. & Wilson, W. E., 1982. *Astr. Astrophys. Suppl. Ser.,* **47,** 1.
Haslam, C. G. T., Wilson, W. E., Graham, D. A. & Hunt, G. C., 1974. *Astr. Astrophys. Suppl. Ser.,* **13,** 369.
Haslam, C. G. T., Klein, U., Salter, C. J., Stoffel, H., Wilson, W. E., Cleary, M. N., Cooke, D. J. & Thomasson, P., 1981. *Astr. Astrophys.,* **100,** 209.
Hayakawa, S., Kato, T., Nagase, S., Yamashita, K. & Tanaka, Y., 1979. *Publs astr. Soc. Japan,* **31,** 71.
Hogg, D. C., 1959. *J. Appl. Phys.,* **30,** 1417.
Howell, T. F., 1970. *Astrophys. Lett.,* **6,** 45.
Howell, T. F. & Shakeshaft, J. R., 1966. *Nature,* **210,** 1318.
Howell, T. F. & Shakeshaft, J. R., 1967. *Nature,* **216,** 753.
Kallas, E., Reich, W. & Haslam, C. G. T., 1983. *Astr. Astrophys.,* **128,** 268.
McCammon, D., Burrows, D. N., Sanders, W. T. & Kraushaar, W. L., 1983. *Astrophys. J.,* **269,** 107.
McKee, C. F. & Ostriker, J. P., 1977. *Astrophys. J.,* **218,** 148.
Milogradov-Turin, J., 1984. *Mon. Not. R. astr. Soc.,* **208,** 379.
Milogradov-Turin, J. & Smith, F. G., 1973. *Mon. Not. R. astr. Soc.,* **161,** 269.
Pauliny-Toth, I. I. K. & Shakeshaft, J. R., 1962. *Mon. Not. R. astr. Soc.,* **124,** 61.
Pelyushenko, S. A. & Stankevich, K. S., 1969. *Soviet Asr.,* **13,** 223.
Phillipps, S., Kearsey, S., Osborne, J. L., Haslam, C. G. T. & Stoffel, H., 1981. *Astr. Astrophys.,* **103,** 405.
Purton, C. R., 1966. *Mon. Not. R. astr. Soc.,* **133,** 463.
Reich, W., 1982. *Astr. Astrophys. Suppl. Ser.,* **48,** 219.
Reich, P. & Reich, W., 1986. *Astr. Astrophys. Suppl. Ser.,* **63,** 205.
Sironi, G., 1974. *Mon. Not. R. astr. Soc.,* **166,** 345.
Spoelstra, T. A. Th., 1972. *Astr. Astrophys.,* **21,** 61.
Strong, A. W., 1977. *Mon. Not. R. astr. Soc.,* **181,** 311.
Troland, T. H. & Heiles, C., 1982. *Astrophys. J.,* **252,** 179.
Turtle, A. J. & Baldwin, J. E., 1962. *Mon. Not. R. astr. Soc.,* **124,** 36.
Turtle, A. J., Pugh, J. F., Kenderdine, S. & Pauliny-Toth, I. I. K., 1962. *Mon. Not. R. astr. Soc.,* **124,** 297.
Webster, A. S., 1974. *Mon. Not. R. astr. Soc.,* **166,** 355.
Webster, A. S., 1975. *Mon. Not. R. astr. Soc.,* **171,** 253.
Webster, A. S., 1978. *Mon. Not. R. astr. Soc.,* **185,** 107.
Weiss, D., 1980. *Ann. Rev. Astr. Astrophys.,* **18,** 489.
Wilkinson, A. & Smith, F. G., 1974. *Mon. Not. R. astr. Soc.,* **167,** 593.
Willis, A. G., Oosterbaan, C. E., Le Poole, R. S., de Ruiter, H. R., Strom, R. G., Valentijn, E. A., Katgert, P. & Katgert-Merkelijn, J. K., 1977. In: *IAU Symp. No. 74, Radio Astronomy and Cosmology,* p. 39, ed. Jauncey, D. L., D. Reidel, Dordrecht, Holland.